The Astrophysical Journal, 869:149 (13pp), 2018 December 20 https://doi.org/10.3847/1538-4357/aaee7c

Magnetic Fields on the Flare Star Trappist-1: Consequences for Radius Inflation and Planetary Habitability

D. J. Mullan[1], J. MacDonald[1], S. Dieterich[2], and H. Fausey[1]
[1] Dept. of Physics and Astronomy, University of Delaware, Newark, DE 19716, USA
[2] Dept. Terrestrial Magnetism, Carnegie Institution of Washington, Washington, DC 20015, USA
Received 2018 September 14; revised 2018 October 31; accepted 2018 November 1; published 2018 December 20

Abstract

We construct evolutionary models of Trappist-1 in which magnetic fields impede the onset of convection according to a physics-based criterion. In the models that best fit all observational constraints, the photospheric fields in Tr-1 are found to be in the range 1450–1700 G. These are weaker by a factor of about 2 than the fields we obtained in previous magnetic models of two other cool dwarfs (GJ 65A/B). Our results suggest that Tr-1 possesses a global poloidal field that is ∼100 times stronger than the Sun's global field. In the context of exoplanets in orbit around Tr-1, the strong poloidal fields on the star may help to protect the planets from the potentially destructive effects of coronal mass ejections. This, in combination with previous arguments about the beneficial effects of flare photons in the ultraviolet and visible portions of the spectrum, suggests that conditions on Tr-1 are not necessarily harmful to life on a planet in the habitable zone of Tr-1.

Key words: magnetic fields – stars: activity – stars: flare – stars: individual (Trappist-1)

1. Introduction

Trappist-1 (Tr-1) is an M8 dwarf star with an estimated age reported by Burgasser & Mamajek (2017, hereafter BM17) to be 7.6 ± 2.2 Gyr. The star is surrounded by at least seven exoplanets, of which three are believed to lie in the habitable zone (HZ) and are therefore of interest in the context of extraterrestrial life. Moreover, with an age that (according to BM17) is at least as old as the Sun, there has been at least as much time for life to emerge on a Tr-1 planet as in the case of the Earth. We shall return to a discussion of the age of Tr-1 in the context of rotation and spot coverage in Section 2 below.

According to BM17, the stellar radius ($0.121 \pm 0.003\, R_\odot$) is inflated relative to the predictions of solar-metallicity evolutionary models for a star with mass $0.08\, M_\odot$ by 8%–14%. However, these percentage inflations in the radius depend sensitively on the value one chooses for the stellar mass: Van Grootel et al. (2018) concluded that the mass of Tr-1 is not as small as BM17 suggested. Instead, Van Grootel et al. (2018) cited a mass of $0.089 \pm 0.006\, M_\odot$: in such a case, the percentage radial inflation, while still present, would not be as large as the values reported by BM17. The occurrence of an empirically inflated radius on Tr-1 is the principal reason why we undertake the magnetic modeling of Tr-1 described in Section 3 below.

Vida et al. (2017) reported on a study of 42 flares on Tr-1 detected by the *Kepler* spacecraft. Because of the possible dangers to living organisms that might be posed by the effects of flares on exoplanets in orbit around Tr-1, Vida et al. stated (in their abstract) that the flares "make these (exoplanets) less favorable for hosting life." And, in the title of their paper, Vida et al. (2017) explicitly included the question "Unsuited for Life?"

In the present paper, our goal is to reexamine this question of suitability for life on a Tr-1 planet using information we obtain from models of the star that include the structural effects of magnetic fields.

In Section 2, we summarize the information that can be extracted from photometric data concerning the properties of magnetic features on the surface of Tr-1. In Section 3, we present the principal results of this paper, namely, quantifying the internal structure of Tr-1 in the context of a magnetoconvective model. This model leads to the key physical quantity of interest in the present paper, i.e., the strength of the magnetic field on the surface of Tr-1. In Section 4, we discuss our estimates of the surface magnetic field in terms of the global components of the field on Tr-1. In Section 5, we consider some quantitative details as to how the surface magnetic fields on Tr-1 contribute to flaring activity on that star. In Section 6, we consider the appropriateness of making comparisons between the magnetic fields in stars that differ in internal structure. In Sections 7 and 8, we reexamine the question of suitability for life on a Tr-1 planet from two points of view: (i) mass ejections (Section 7) and (ii) photons (Section 8). Conclusions are discussed in Section 9.

2. Rotational Period and Variability: Spots and Faculae

The rotational period of Tr-1 is variously reported as 3.3 days (Luger et al. 2017; Vida et al. 2017), 1.40 days (Gillon et al. 2016), and 0.819 days (Roettenbacher & Kane 2017). These rotation periods are shorter than the Sun's by factors of 10–30; i.e., the angular velocity Ω in Tr-1 exceeds Ω(Sun) by 10–30. Kippenhahn (1973) suggested that the strength of a dynamo field B should increase as Ω increases according to $B \sim \Omega^x$, where $x = 1$ or 1.5. If such scalings are relevant to Tr-1, then the dynamo field strength on Tr-1 could exceed that in the Sun by factors that are at least as large as 10–30 and perhaps as large as 30–160. In the present paper, we examine this possibility quantitatively from the perspective of stellar structure by constructing magnetoconvective models of Tr-1.

It is important to note that Luger et al. (2017), using an 80 day segment of data from the *Kepler K2* mission, reported a light curve for Tr-1 that suggests (to the eye) that the most prominent photometric features appear to be excursions away from the overall average brightness toward larger brightnesses. And the amplitudes of the excursions are, on average, seen (by visual inspection) to be at the ∼1% level. This is in contrast to

other cool stars in two respects: (i) qualitatively, in the presence of cool starspots, the most prominent features in the light curve are well-defined excursions to smaller brightnesses; and (ii) quantitatively, the amplitudes of the excursions on spotted stars can be as large as 30%–40% (e.g., Bopp & Evans 1973; Strassmeier 1999). In the Sun, excursions to larger brightnesses are associated with localized bright features labeled photospheric faculae (e.g., Bray & Loughhead 1964, hereafter BL64). Rackham et al. (2018) quantified the separate contributions of spots and faculae to the photometric variations in Tr-1: they concluded that spots occupy 8% of the surface area, while faculae occupy 54%. The analysis of Rackham et al. assumed that the spots and faculae are long-lived features. Relaxing the assumption of longevity, Morris et al. (2018) analyzed the Tr-1 variability in terms of shorter-lived surface features that they called "bright starspots." Morris et al. suggested that the bright starspots have radii $R_{\rm spot}$ of about 0.004 $R_\star$; with $R_\star = (0.121 \pm 0.003)\,R_\odot = 8.5 \times 10^9$ cm, we find that the spots have linear radii of about 300 km. Such radii are reminiscent of facular elements on the Sun, which have linear dimensions of <300 km and are magnetic flux tubes located in the dark intergranular lanes. In the Sun, granules have horizontal dimensions of order 1000 km, and the dark intergranular lanes are smaller than this by a factor of a few. In view of this, we suggest that the "bright starspots" mentioned by Morris et al. may be considered as analogs of faculae, i.e., individual magnetic flux ropes in which the reduced density allows one, when viewing at a finite angle from the vertical, to see downward to the hot walls of the flux rope in deeper layers (Spruit 1976).

In fact, in the Sun, it is observed that the radiant flux varies during the solar cycle in such a way that when sunspots are most abundant, the solar luminosity is larger than average (e.g., Radick et al. 2018). This indicates that the flux excesses from faculae in the Sun more than compensate for the flux deficits in sunspots. Thus, the Sun is a star where the temporal variability associated with the activity cycle is dominated by faculae. Radick et al. (1998) reported that, depending on the intensity of chromospheric activity, there is a transition from facular-dominated variability to spot-dominated variability. The sense of the transition is that stars where the activity level is lower tend to exhibit facular-dominated variability (such as the Sun), whereas more active stars have variability that is dominated by spots. These conclusions of Radick et al. (1998) were reinforced by Shapiro et al. (2014), who also extended the properties to include the effects of different angles between the rotation axis and the line of sight.

Given the predominance of facular variability in Tr-1, it seems plausible to conclude that Tr-1 resembles the Sun to the extent that both can be assigned to the "low-activity set" of magnetically active stars.

On the other hand, the "low-activity" label for Tr-1 has recently been challenged by Dmitrienko & Savanov (2018, hereafter DS). Using the same *Kepler K2* data set as Luger et al. (2017) but reduced using different algorithms, DS found that the amplitude of Tr-1 light excursions was not 1% (as estimated above), but 2.6%–3.1%. Interpreting these fluctuations in terms of spots with certain temperatures (160 K cooler than the photosphere), DS calculated that a fractional area $S = 5\%$–6% of the surface of Tr-1 is covered by spots. By comparing with their previous estimates of S values in a sample of 1570 M dwarfs with known ages, DS claimed that Tr-1 is a high-activity star with an "S-age" of less than 200 Myr. Such a young age is problematic for stellar evolution theory; as will be seen in Figure 1 below, a star with an age of 200 Myr and a mass of 0.08–0.09 $M_\odot$ would still be in its pre-main-sequence phase of evolution, with properties that would deviate by many σ from the empirical data for Tr-1. Moreover, if the age is really as low as 200 Myr, the interest in Tr-1 as regards the emergence of life would diminish considerably; on Earth, it is estimated that some 200 Myr had to elapse before the first life emerged (e.g., Dodd et al. 2017). However, we note that in Figure 4 of DS, there is considerable scatter in the S-age data. In fact, within the error bars plotted by DS for Tr-1, there are several M dwarfs with S-ages of more than 1 Gyr; the two oldest of these have S-ages of 2.6–3.1 Gyr. Furthermore, DS also referred to X-ray data on Tr-1 that suggest an age of 2 ± 1 Gyr. They did not explain how to reconcile the 10-fold discrepancy between X-ray age and their claim of 0.2 Gyr for the S-age. In the context of the evolutionary calculations to be reported in the present paper, we note that stars with masses in the range 0.08–0.09 $M_\odot$ reach the main sequence in times of 0.5–0.8 Gyr. Once on the main sequence, their lifetimes ($\sim M/L \sim 1/M^{2-3}$) are $\geqslant 10^3$ Gyr. With such long lifetimes, the differences in L and R between a star with an age of 2–3 Gyr and a star with an age of 5–7 Gyr are negligible on the scales of our Figures 1–5. Hence, our results can be applied without significant error to the empirical data, whether the "true" age of Tr-1 has the value reported by BM17 or the X-ray age reported by DS.

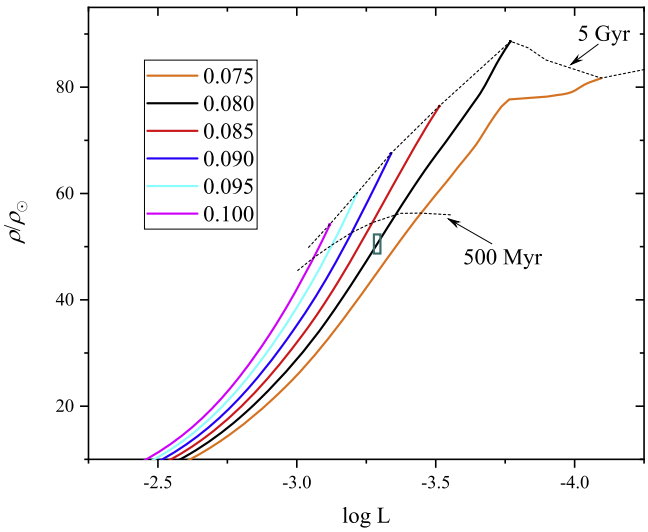

Figure 1. Evolutionary tracks of nonmagnetic stellar models in the log (luminosity)–log(mean density) plane. The mass on a track of a given color is listed in the inset (in units of $M_\odot$). The dotted lines in the figure are isochrones for models of ages of 500 Myr and 5 Gyr. The empirical location of Tr-1 is shown by the dark cyan rectangle. Solar units are used for L and ρ.

3. Evolutionary Models of Tr-1: Derivation of Surface Magnetic Field Strength

The possibility that Tr-1 has an empirical radius that exceeds the radius of a standard (nonmagnetic) model of a star with a specified mass suggests that it is worthwhile to explore the case of a stellar model in which a global magnetic field is present. Such a model can be derived based on a quantitative formulation of the physics involved in a low-mass star where the presence of a vertical magnetic field in an electrically

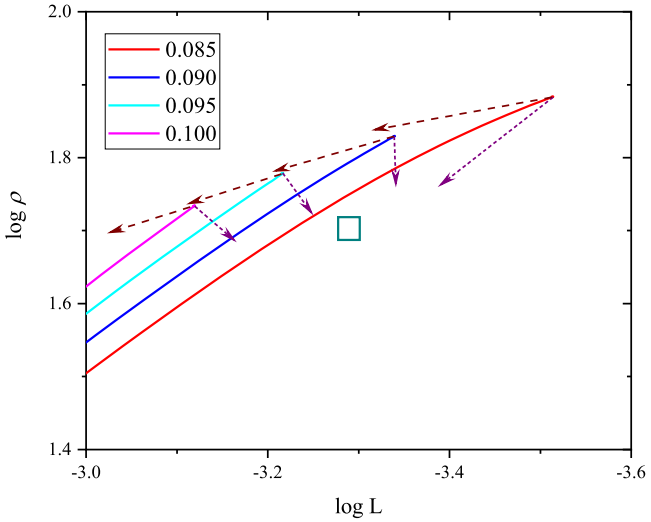

Figure 2. Evolutionary tracks of low-mass stars plotted in the log L–log ρ plane. Notation is the same as in Figure 1. The long-dashed brown and short-dashed purple arrows show the directions of the model main-sequence shifts when Y and Z (respectively) are independently increased. The lengths of the arrows correspond to increments of log Y and log Z of 0.1 and 0.3, respectively. The empirical location of Tr-1 is shown by the dark cyan rectangle.

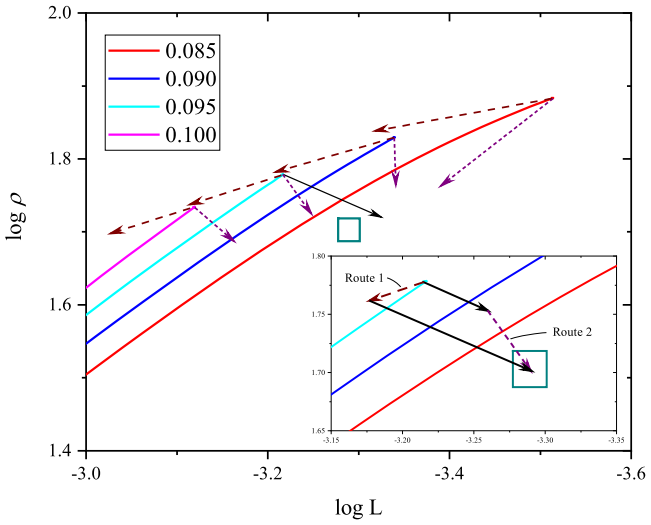

Figure 3. Same as Figure 2 but with the addition of a solid black line with an arrowhead in the main part of the figure. This shows the direction of the shift in the location of the main sequence of a 0.095 $M_{\odot}$ model due solely to inclusion of the magnetic inhibition of convection in the absence of any changes in Y or Z.

conducting medium impedes the onset of convection (Mullan & MacDonald 2001; MacDonald & Mullan 2012, 2014, 2017a).

3.1. The Observational Data

In this subsection, we present the constraints on stellar modeling that are set solely by observational data: i.e., we do not consider in this subsection any results that depend on stellar models.

The metallicity has been determined from near-infrared spectroscopy (Gillon et al. 2016) to be near solar, [Fe/H] = $+0.04 \pm 0.08$. From a comprehensive analysis of empirical age constraints, BM17 determined that Tr-1 has an age of 7.6 ± 2.2 Gyr. From analysis of the transit light curves,

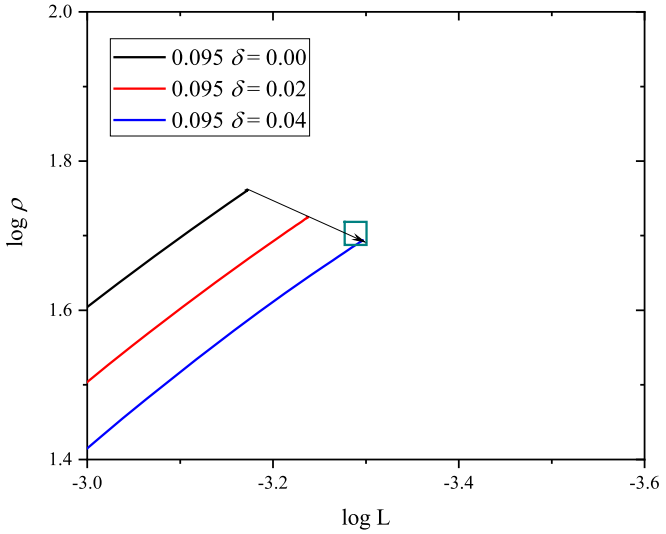

Figure 4. Preliminary evolutionary tracks of magnetic models in the luminosity–mean density plane. The uppermost continuous track refers to a nonmagnetic model with mass 0.095 $M_{\odot}$. This line ends when the star reaches the main sequence. In this case, the magnetic inhibition parameter δ has a value of zero. With increasing magnetic field strength, the main-sequence location shifts to the lower right along the thin black line with an arrowhead. The tip of the arrow shows the main-sequence location when the magnetic field is such that $\delta = 0.04$ in the stellar photosphere. Also plotted is the evolutionary track of a magnetic model with $\delta = 0.02$. The location of Tr-1 is shown by the dark cyan rectangle. In this figure, the term "preliminary" means that we use the GT criterion (Equation (1)); i.e., the electrical conductivity is assumed to be infinite. In this limit, the fields are maximally effective for impeding the onset of convection.

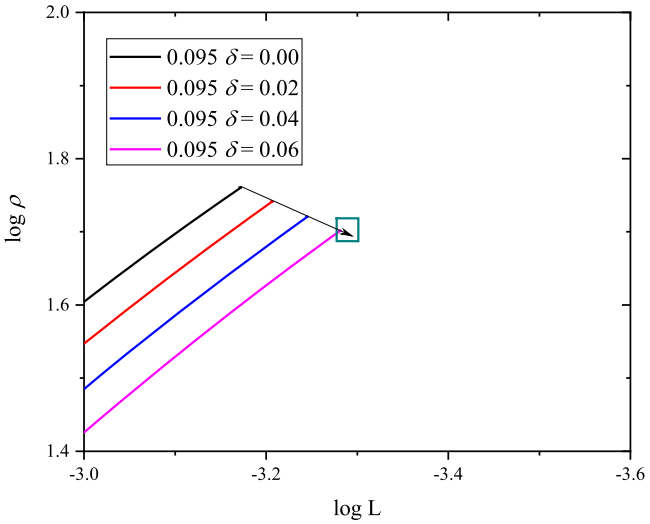

Figure 5. Same as Figure 4, except that here, the effects of finite electrical conductivity on magnetoconvection have been included in the models.

Delrez et al. (2018) determined the mean stellar density to be $\rho = 51.1^{+1.2}_{-2.4}$ in units of the mean density of the Sun. From analysis of the optical data for Tr-1, Van Grootel et al. (2018) determined the parallax to be 82.4 ± 0.8 mas; i.e., the distance to Tr-1 is 12.14 ± 0.12 pc. This distance is considerably more precise than the distance obtained by Costa et al. (2006), although the mean values of the distance overlap within the error bars. Using the spectral energy distribution of Filippazzo et al. (2015), Van Grootel et al. (2018) found the luminosity of Tr-1 to be $L = (5.22 \pm 0.19) \times 10^{-4} L_{\odot}$.

This set of data is insufficient by itself to determine the stellar mass or radius. Therefore, we have applied the method of Dieterich et al. (2014; see also MacDonald et al. 2018) to determine the luminosity and effective temperature of Tr-1 from published photometry (Filippazzo et al. 2015). We find, based on the parallax measurement of Van Grootel et al., that $L = (5.14 \pm 0.14) \times 10^{-4} L_{\odot}$ and $T_{\rm eff} = 2519 \pm 51$ K. The corresponding radius value is $R = 0.1190 \pm 0.0051 R_{\odot}$. Using this radius with the mean density measurement from Delrez et al., we find that the stellar mass is $M = 0.0858 \pm 0.0114 M_{\odot}$.

From analysis of the FeH absorption band, Reiners & Basri (2010) determined that Tr-1 has a magnetic field averaged over the visible surface of $Bf = 600^{+200}_{-400}$ G.

Using a number of empirical age constraints from kinematics, rotation, magnetic activity, lithium absorption, position in the color–absolute magnitude diagram, average density, surface gravity features, and metallicity, BM17 determined that Tr-1 has an age of 7.6 ± 2.2 Gyr.

3.2. Previous Modeling

Using only the mean stellar density and their luminosity value as constraints, Van Grootel et al. (2018) determined from their stellar modeling that the stellar mass would need to be $0.081 \pm 0.003 M_{\odot}$, and the age would then be 450 ± 55 Myr. The corresponding model radius and effective temperature are $0.117 \pm 0.002 R_{\odot}$ and 2555 ± 25 K. Because this age is in clear conflict with that found by BM17, Van Grootel et al. also applied only the luminosity and age constraints to their stellar evolution modeling. In this case, agreement is found for a stellar mass of $0.089 \pm 0.003 M_{\odot}$ and an age between 2 and 15 Gyr. The corresponding model radius and effective temperature are $0.114 \pm 0.002 R_{\odot}$ and 2595 ± 30 K. No reasonable fit is found at solar metallicity when the constraints from luminosity, age, and density are applied together. The stellar density at $\sim 0.09 M_{\odot}$ is found to be much higher than the value measured from transits because the model stellar radius is too low. Van Grootel et al. pointed to "the usual suspects" for this radius anomaly: (1) the presence of a strong magnetic field causing the stars to inflate by inhibiting convective energy transport (Mullan & MacDonald 2001) and/or by creating surface spots (Chabrier et al. 2007) or (2) higher than solar metallicity causing the star to inflate due to larger opacity (Feiden & Chaboyer 2014).

In the present paper, we report on a quantitative investigation that seeks to interpret the empirical inflation of the radius of Tr-1 in the context of magnetic inhibition of the onset of convective energy transport.

3.3. Magnetoconvective Modeling

Although our model for magnetoconvection was first described in Mullan & MacDonald (2001), improvements have been added in the intervening years. A description of the current model is provided by MacDonald et al. (2018). In the latter paper, we compared the theoretical magnetic field strengths required to give the observed radius inflations of the components of the M-dwarf binary GJ 65 with the field strengths determined by Kochukhov & Lavail (2017) and Shulyak et al. (2017). Other aspects of our stellar evolution code are described in MacDonald & Gizis (2018).

We have made one important modification to the method described in MacDonald et al. (2018) for construction of magnetic stellar models for Tr-1. As a first step in our method, we construct nonmagnetic models using boundary conditions from atmosphere calculations based on the T–τ relation of Krishna Swamy (1966, hereafter KS). Our goal is to have the KS models match the photospheric properties of nonmagnetic models that use boundary conditions from BT-Settl atmosphere models (Allard et al. 2012a, 2012b; Rajpurohit et al. 2013). This requires us to adjust the mixing-length parameter, α, in the KS atmosphere calculations. In MacDonald et al. (2018), for reasons of simplicity, a single value for α appropriate for low-mass main-sequence models, $\alpha = 0.7$, was used. In the present paper, we use the value of α that gives the best match to the BT-Settl boundary conditions for a given log g and $T_{\rm eff}$.

Our adopted magnetic field profile depends on two parameters: a magnetic inhibition parameter, δ, and a magnetic field ceiling, $B_{\rm ceil}$. The magnetic inhibition parameter, which was first introduced by Gough & Tayler (1966, hereafter GT), is a local parameter defined by

$$\delta = \frac{B_v^2}{4\pi\gamma P_{\rm gas} + B_v^2}, \quad (1)$$

where B_v is the vertical component of the magnetic field, $P_{\rm gas}$ is the gas pressure, and γ is the ratio of specific heats. In the original GT criterion, convective stability is ensured as long as the radiative gradient $\nabla_{\rm rad}$ does not exceed $\nabla_{\rm ad} + \delta$, where $\nabla_{\rm ad}$ is the adiabatic gradient. In the original GT paper, the primary interest was in the conditions that exist in the Sun. In such an environment, the temperatures of the gas in which magnetic fields and convection interact are high enough that the electrical conductivity has a large value that can (without significant error) be considered to be in effect infinite in the context of the ambient convective cells. However, in stars that are clearly cooler than the Sun (such as GGJ65A/B and Tr-1), the assumption of infinite electrical conductivity is no longer valid. At temperatures of 2600 K or less, the question that plays a key role in the field–gas interaction is the following: in the course of the (finite) time period required for material in a convective cell to complete one circulation of the cell, how effectively can the magnetic fields become "unfrozen" and "slip" through the gas? In cases where the "slippage" is large enough to amount to a significant fraction of the linear size of a convective cell, a magnetic field of a given strength is less effective at impeding the onset of convection than such a field would be in the Sun (MacDonald et al. 2018). To quantify the effects of finite conductivity, we replace the original GT criterion with a modified "GTC criterion" (MacDonald & Mullan 2009). Our GTC code includes the effects of field-line "slippage" through the mostly neutral gas near the photosphere (MacDonald & Mullan 2017a) and allows for deviations from ideal gas behavior (Mullan & MacDonald 2010).

3.4. Models that Do Not Include Magnetic Effects

Before considering models that include the effects of magnetic fields on stellar structure, we explore the possibility that the observed low density of Tr-1 could be the result of higher-than-solar heavy-element abundances. We begin by presenting results for models that have the same abundances as

the BT-Settl atmosphere models, i.e., the solar photospheric abundances derived by Caffau et al. (2011). The mass fractions of hydrogen, helium, and heavy elements are $X = 0.7321$, $Y = 0.2526$, and $Z = 0.0153$, respectively. The models have masses that cover a range that is consistent with our temperature determination, i.e., 0.075–0.100 $M_{\odot}$, in increments of 0.005 $M_{\odot}$. We show in Figure 1 evolutionary tracks in the luminosity–mean density plane with the masses (in units of solar mass) shown in the legend. The dotted lines in Figure 1 display the isochrones for our models, one with an age of 500 Myr and the other with an age of 5 Gyr. The empirical location of Tr-1 in this plane is shown by the dark cyan rectangle.

The fact that, in Figure 1, the 0.080 $M_{\odot}$ track (black line) passes through the empirical rectangle for Tr-1 might, at first sight, lead us to conclude that the mass quoted by BM17 (0.080 $M_{\odot}$) could be a good fit to the empirical data. That conclusion might be correct if we were to restrict our consideration to the empirical values of only two quantities (L and ρ) and disregard other parameters. However, such a conclusion is ruled out when we also take into account another parameter, namely, the age of Tr-1. It is important to note that the empirical rectangle for Tr-1 in Figure 1 is situated in a position that lies definitely below the 500 Myr isochrone; such a position would require that Tr-1 have an age that is less than 500 Myr. That age would be much too young to be consistent with the age of Tr-1 as reported by BM17, a conclusion that was also reached by Van Grootel et al. (2018). For completeness, we should mention that an age of less than 500 Myr could be consistent with the S-age quoted by DS; however, we have already mentioned (see Section 2 above) that the DS estimate of the S-age could be too small by an order of magnitude, while a second age estimate by DS (based on X-rays) is also too long (by an order of magnitude) to be consistent with the quoted S-age. In view of these properties, in what follows, we will focus on Tr-1 models that are on the main sequence.

We next explore the possibility that the mass, age, luminosity, and mean density constraints could be simultaneously satisfied by nonmagnetic models in which the abundances of the elements take on different numerical values. Because the BT-Settl atmospheres (which do not incorporate magnetic fields) are available for only a few sets of abundances, we perform a differential analysis using models computed with a simple Eddington boundary condition. Figure 2 shows the effects of increasing Y (alone) or Z (alone) on the location of the model main-sequence phase. Increasing Y while keeping Z fixed is equivalent to increasing the stellar mass while retaining Y and Z at their original values.

We see from Figure 2 that there is a narrow range of mass, between 0.090 and 0.095 $M_{\odot}$, for which the main sequence could, in principle, be shifted to a location consistent with the empirical rectangle in the L–ρ plane by simply increasing Z while keeping Y fixed. In fact, if we were permitted to increase Z to any value whatsoever, no matter how large, the empirical rectangle could likely be replicated. However, the question that is of quantitative relevance here is: how much would Z have to be increased in order to obtain consistency with the empirical rectangle? The answer is found to be as follows. The minimum value of Z for which our models would agree with the empirical rectangle at the 1σ level is $Z = 0.036$. The corresponding Z/X ratio is 0.051. Determining the correspondence with the observed [Fe/H] $= +0.04 \pm 0.08$ (Gillon et al. 2016) requires knowledge of the solar Z/X ratio; this remains a hot topic of debate, with values ranging from 0.0165 (Asplund et al. 2006) to 0.0274 (Anders & Grevesse 1989) to a helioseismologically preferred value of 0.0233 (Antia & Basu 2006). A value of $Z/X = 0.051$ corresponds to [Fe/H] = 0.27–0.49, which is discrepant by 2.9σ–5.6σ from the mean value reported by Gillon et al. (2016). These discrepancies are so large that we conclude that the radius inflation observed in Tr-1 is unlikely to be solely due to high metallicity.

The conclusion that metal abundances alone cannot explain the radius inflation in low-mass stars that are metal-poor has already been discussed in earlier work on the metal-poor binary CM Dra (MacDonald & Mullan 2012). We were able to strengthen this conclusion by comparing CM Dra to a binary that has similar masses as CM Dra but with a metal-rich composition (KOI 126). The contrast was striking: in KOI 126, the inflated radii were found to agree with a model with enhanced metals alone, and there was no need to call upon magnetic effects to fit the data. But for CM Dra, with its low metal abundance, we could not explain the inflated radii on the basis of enhanced metals. Magnetic fields were, however, found to be adequate to the task.

3.5. Results of Magnetoconvective Modeling of Tr-1

Now we turn to models in which the effects of magnetic fields are explicitly included in the criterion for the onset of convection. As shown by Mullan & MacDonald (2001), two principal characteristics emerge from magnetoconvective models: (i) the radius of a magnetic model with a given mass is larger than that of a nonmagnetic model with the same mass (or, equivalently, the mean density of a magnetic model is smaller than that of a nonmagnetic model with the same mass), and (ii) the effective temperature of the magnetic model is smaller than that of the nonmagnetic model with the same mass. In the process of computing our magnetoconvective models, we vary the strength of the surface magnetic field in order to achieve the following. Given the ages that have been determined by BM17, what value of the field strength is required to give consistency not only with the mean density but also with the empirical values of radius, effective temperature, and luminosity?

Figure 3 is similar to Figure 2, except that, in the main part of the figure, we have added a solid black line with an arrowhead. The tip of the arrow illustrates the location of a nonmagnetic main-sequence model of mass 0.095 $M_{\odot}$ that shifts when a magnetic field of a certain strength B_v is included in the stellar model. In the case of the model illustrated by the arrow, we have modeled magnetoconvection according to the GT criterion (see Equation (1)). We stress that the black arrow in the main part of Figure 3 refers to a model in which the only difference from the nonmagnetic main-sequence model of mass 0.095 $M_{\odot}$ is the inclusion of a nonzero value of B_v; there are no alterations to Y or Z.

Now that we have determined the shifts in the main-sequence location by changing one parameter (either Y, Z, or B_v), we can also determine how simultaneous changes in more than one parameter shift the main-sequence location. The inset in Figure 3 shows two possible routes for shifting the 0.095 $M_{\odot}$ main-sequence model so that our model results lie in the empirical error box for Tr-1. Along the dashed line labeled Route 1, Z is kept fixed at $Z = 0.0153$, but Y is increased to

$Y = 0.2796$ (as shown by the dashed brown arrow in the inset). In this case, the value of B_v required in order to reach the empirical rectangle is relatively large, as illustrated by the longer black line in the inset that starts at the tip of the brown arrow and ends inside the empirical rectangle. Along the dashed line labeled Route 2, Y is fixed at $Y = 0.2526$, but Z is increased to $Z = 0.0296$. In this case, the dashed purple arrow (due to enhanced Z) moves in the direction of the empirical rectangle in such a way that when we include magnetoconvection, a shorter black arrow, when vectorially added to the purple arrow, enables us to reach the empirical rectangle. The shorter length of the black arrow in Route 2 indicates that a weaker magnetic field will fit the empirical rectangle than in Route 1. In general, when we construct magnetic models with a chosen value of Z, the value we obtain for B_v should be considered as an upper limit on the field strength if the star is actually more metal-rich than we assume in our models. Conversely, if the star is actually more metal-poor than we assume in our models, then our result for B_v can be considered as setting a lower limit on the field strength.

Alternatively, agreement with the observations can also be obtained for the Caffau et al. (2011) composition models by including only the magnetic effects if the mass of the model is $\sim 0.097\ M_\odot$ (results for this case are not shown).

In order to calculate our magnetic models for Tr-1, in line with our recent modeling (MacDonald & Mullan 2017b), we set the ceiling on field strength to be $B_{\rm ceil} = 10$ kG. This choice of $B_{\rm ceil}$ is based on the maximum magnetic field strength found in simulations of dynamos in low-mass stars (Browning 2008; Yadav et al. 2015). We show in Figure 4 a preliminary set of our magnetoconvective evolutionary tracks in the luminosity–mean density plane. In Figure 4, all tracks have mass $0.095\ M_\odot$ and composition $Y = 0.2796$ and $Z = 0.0153$. The differences between tracks are due to differences in magnetic field strength, as shown by the different numerical values of the magnetic inhibition parameter δ (see Equation (1)). In this preliminary set of tracks, we choose not to include the effects of finite electrical conductivity in our magnetoconvective models: the magnetic fields are assumed to be perfectly coupled to the gas and therefore maximally effective for impeding the onset of convection. Despite the preliminary nature of the tracks, these models clearly show that magnetic effects lead to inflated radii and therefore could be relevant in our search for a model that fits Tr-1.

For consistency with all of the observational data (luminosity, mean density, and age), the results in Figure 4 show that the magnetic inhibition parameter δ (see Equation (1)) must have a value that lies in the range $\delta = 0.03$–0.04. Combining these numerical values for δ with the gas pressure in the photosphere of each model, we find that the corresponding vertical magnetic field strengths B_v in the photosphere of Tr-1 would be $B_{\rm ps} \sim 1100$–1300 G.

The assumption of infinite electrical conductivity that was used in calculating the preliminary tracks shown in Figure 4 cannot be justified in Tr-1. Two lines of argument can be presented to indicate that the effects of finite conductivity play a role in stars that are close to (or below) the lower end of the main sequence. First, the slope of the flare frequency distribution changes significantly among the coolest flare stars (Mullan & Paudel 2018): the change in slope can be attributed quantitatively to the onset of finite conductivity. Second, MacDonald et al. (2018) demonstrated quantitatively that at the low temperatures ($T_{\rm eff} \sim 2700$–2800 K) that exist in the surface layers of GJ 65A and GJ 65B, the presence of finite electrical conductivity allows the mostly unionized gas to drift significantly through the magnetic field lines. That is, the magnetic field does not have "as much of a hold on" the gas as it would have in a medium where electrical conductivity is infinite. In such cases, in calculating a magnetoconvective model, we do not rely on the GT criterion but on the GTC criterion (see Section 3.3 above). Since the effective temperature of Tr-1, $T_{\rm eff} \sim 2500$ K, is even lower than those of GJ 65A/B, we expect that the effects of finite electrical conductivity are even more significant for Tr-1. Therefore, in order to replicate a given empirical inflation of the radius, the field strength in Tr-1 needs to be larger than it would be if electrical conductivity were infinite. To quantify this in the context of Tr-1, we show in Figure 5 (which has the same format as Figure 4) the values of δ that are needed in order to be consistent with the empirical error rectangle. In this case, we now find that the magnetic inhibition parameter must have larger numerical values, namely, in the range $\delta = 0.05$–0.07. Combining these values with the gas pressure in the photosphere ($\sim 2 \times 10^6$ dyn cm^{-2}), we find that the corresponding vertical field strengths in the photosphere of Tr-1 are $B_{\rm ps} \sim 1450$–1700 G. As expected, these fields are stronger than the fields that would suffice to replicate the empirical inflation (in an idealized model) if the electrical conductivity were in effect infinite (see Figure 4).

4. Magnetic Fields in Tr-1: Poloidal and Toroidal Components

It is important to note that, when we use the GT (or GTC) criteria to obtain a best-fit magnetoconvective model of a star, the principal result that emerges is a numerical value of the parameter δ at the surface of the star. A key aspect of δ is that it depends on a particular component of the magnetic field, namely, the vertical component B_v of the field that threads through a convection cell. Therefore, the values of $B_v = 1450$–1700 G obtained above for Tr-1 refer to an average vertical field strength over the surface of the star. How should we interpret these field strengths in the context of the global field distribution of magnetic field that exists in the near-surface layers of a low-mass star such as Tr-1? To address this, it is convenient to consider how any divergence-free vector quantity (e.g., a magnetic field) can usefully be decomposed in a spherical system into two components: poloidal and toroidal.

4.1. Poloidal Fields

In the Sun, the poloidal component includes a global dipole, which is most easily observed in and near the polar regions. This component can be identified in coronal images at all stages of the solar cycle, although it is easier to identify at solar minimum. For example, see Habbal et al. (2010, their Figure 1), where remarkable images are reported of an eclipse that occurred during the deep solar minimum of 2008. Near the poles of the Sun, the field lines on the solar surface are essentially vertical, i.e., radial: $B_{\rm ps} \approx B_v \approx B_r$. Because of this, attempts to derive the Sun's surface field at the poles by observations from Earth are hampered by serious foreshortening. Instead, in situ measurements of the radial field in interplanetary space $B_{r,i}$ can be made in a solar wind stream that emerges from a coronal hole. Conservation of magnetic

flux requires that, if the in situ interplanetary stream extends over an area A_i on a Sun-centered sphere, then $B_{r,i}A_i = B_{ss}A_b$, where A_b is the surface area at the base of the coronal hole. In a study of several large solar wind streams observed during the *Skylab* mission, Hundhausen (1977) reported that $B_{\rm ps}$ ranges from 6 to 12 G.

Poloidal fields need not consist only of dipoles. The global dipole is the lowest-order multipole of the magnetic field, with a strength that decreases radially as r^{-3}. Higher-order multipoles of the poloidal field have strengths that decrease faster with radius. As such, the global dipole retains relatively large values out to farther radial distances from the Sun than any higher-order multipole. Therefore, at relatively large altitudes above the surface of the Sun, the corona is threaded predominantly by the global dipole field, with field lines that follow local meridians from one pole to the other. (This global dipole field approximation breaks down beyond a few solar radii. At a certain radial location (the "source surface" of the solar wind), the ram pressure of the solar wind forces the field to open up into a radial topology. However, the "source surface" lies, on average, at a radial location of about 3.25 $R_\odot$ (Koskela et al. 2017), which is far outside the regions where flares occur. Therefore, in the context of flares, we confine our discussion to the global dipole.)

4.2. Toroidal Fields

The toroidal component gives rise to active regions and spots, which are confined to temporary localized regions in lower latitudes. In the Sun, these regions emerge from below the surface, develop into more or less large areas, and eventually decay, on timescales of days or weeks. The strongest values of toroidal fields in the photosphere are observed in sunspot umbrae, where fields up to 2 kG are present in 80% of spots, while 5% of spots have fields exceeding 3 kG (BL64). According to the Babcock (1961) dynamo model, the strong toroidal fields that give rise to sunspots are derived from the poloidal field by means of differential rotation that stretches the poloidal field lines (initially confined to N–S planes) into lines that become progressively aligned in the E–W direction. How strong can the toroidal fields become, in principle? It is difficult to see how the fields can become much stronger than the limit that is set by the gas pressure p_g in the photosphere: if the magnetic pressure $p_m = B^2/4\pi$ were to exceed p_g, a magnetic flux rope would expand horizontally, weakening the value of B until (rough) equipartition is established between p_m and p_g. In fact, given $p_g \sim 1.2 \times 10^5$ dyn cm^{-2} (e.g., Mullan 2009), the equipartition field is predicted to be 1.7–1.8 kG, consistent with the observed fields in the umbrae of most sunspots.

4.3. Which Component of the Field Is Involved in Solar Flares?

When we wish to consider the energy that is released in flares, the strength of the magnetic field in the photosphere is not directly pertinent. The gas in the photosphere is mainly electrically neutral (with a degree of ionization of order 10^{-4}; Mullan 2009). Such a gas is not capable of carrying significant electrical currents. Instead, in the context of flares, we need to consider the magnetic fields in the corona, where the highly ionized plasma allows strong currents to flow. Instabilities in those currents, possibly leading to magnetic reconnection, are believed to be the ultimate source of flare energy (e.g., Alfvén & Carlqvist 1967; Hood & Priest 1979). The toroidal component of the Sun's field gives rise to coronal loops that rise above the surface of an active region: the field strengths in coronal loops can be obtained from observations in X-rays and radio, indicating coronal field strengths ranging from 30 to 583 G (Schmelz et al. 1994). If a flare occurs in a solar active region, it is these coronal fields that ultimately provide the energy. In any particular active region, the foot points of a loop are subject to jostling by convective cells (granules) in the photosphere, and these jostlings can lead to twisting of the field lines. If the twist exceeds a critical value, the field becomes unstable, and a flare starts in the corona (Mullan & Paudel 2018). The energy E that is released in a flare depends on the volume of the loop V and the change in magnetic energy ($\sim B^2$) in the coronal part of the loop: $E \approx V\Delta B^2/8\pi$.

At this point, we ask a question that, at first sight, might seem to be pointless; however, it may set the stage for a subsequent discussion of Tr-1. Does the poloidal field in the Sun play a role in solar flares? The answer is almost certainly "no": the energy density of the poloidal field (of order $\leqslant 1$ erg cm^{-3} on the solar surface at the N and S poles) could, in principle, power a large solar flare ($E \approx 10^{32}$ erg) only if the flare occupied an enormous volume, of order $\geqslant 10^{32}$ cm^3. Such a volume would have to encompass a significant fraction of the entire material contents of the corona, which are contained in a volume V (cor) $= 4\pi R^2 H \approx 4 \times 10^{32}$ cm^3 (where H is the density scale height $\approx 7 \times 10^9$ cm in coronal gas with $T = 10^6$ K). In fact, this estimate of V(cor) is much larger (by a factor of order 10^3) than the volume of the largest solar flare reported by Aschwanden et al. (2015). For this reason, little attention has been paid to considering flares in the poloidal field of the Sun. By contrast, toroidal fields in the Sun can readily supply flare energies even when confined to a limited volume in a single active region.

4.4. Interpreting Our Magnetic Models of Tr-1: Poloidal or Toroidal?

In order to interpret the numerical results of our magneto-convective modeling of a particular star in a realistic manner, we need to determine which component of the magnetic field (poloidal or toroidal) is more relevant in determining the global properties of that star. The toroidal fields are certainly stronger than the poloidal fields, but the toroidal fields are confined to only certain areas of the Sun, and they last only for a finite period of time. Moreover, relative to the surface of the Sun, most of the toroidal fields are horizontal; such fields are much less efficient at interfering with convection than vertical magnetic fields. (A demonstration of this statement can be seen in sunspots, where vertical field lines lead to a cooling of the umbra relative to the photosphere by 1625 K (BL64), whereas the horizontal field lines in the penumbra lead to a cooling of only 285 K (BL64); thus, vertical fields generate 5–6 times more cooling relative to the photosphere than horizontal fields do.) On the other hand, over a large fraction of the northern and southern hemispheres, the poloidal field is mainly vertical and is present at essentially all times (apart from a short time near solar maximum when the poloidal field switches polarity). This leads us to the following hypothesis: the poloidal field is more effective at impeding the onset of convection on a global scale than the toroidal field is.

Can this hypothesis be tested? Yes; in the case of the Sun, we can test it by considering two empirical properties: (i) the

frequencies of p-modes and (ii) the radius of the Sun. As regards item (i), Mullan et al. (2007) used magnetoconvective modeling to determine how the frequencies of p-modes change as the Sun goes from solar minimum to solar maximum. Given the poloidal field that is known to have values in the range 6–12 G (Hundhausen 1977) and the photospheric gas pressure of order 1.2×10^5 dyn cm^{-2} (e.g., Mullan 2009), the numerical value of δ in the polar regions of the Sun's surface is of order 10^{-5}. Models of the Sun with this value of δ allow us to calculate the amount by which the p-mode frequencies alter between solar minimum and maximum (Mullan et al. 2007). The model predicts that p-modes with frequencies of 2000–4000 μHz should shift to higher frequencies at solar maximum by amounts that are several tenths of 1 μHz. These predictions are consistent with empirical frequency shifts. As regards item (ii), our solar models predict that the change in field between solar minimum and maximum should lead to a fractional change in the radius of the Sun of $\Delta R/R \approx (0.7\text{–}3) \times 10^{-5}$, with a smaller radius at solar maximum. Inserting $R = 7 \times 10^5$ km, this predicts that at solar maximum, the solar radius should be smaller by 5–20 km; this is consistent with a report (Kosovichev & Rozelot 2018) that the "seismic radius" of the Sun decreases by 5–8 km at solar maximum.

In view of these checks on our magnetoconvective model as applied to the Sun, we consider that it is appropriate to regard the parameter δ in our Tr-1 model as referring to the poloidal field strength near the poles. As a result, we consider that the fields of 1450–1700 G, which we have derived from magnetoconvective models for Tr-1, are best interpreted as referring to a global dipole field.

Is it possible that our suggestion of a global field of 1450–1700 G on Tr-1 might be inconsistent with the average field strength (600 G) reported by Reiners & Basri (2010) in their observational study of Tr-1? Not necessarily. We may cite the example of another star with a spectral type close to that of Tr-1: the M6.5–M7 star GJ 3622 = 2MASS J10481258–1120082. For this star, Reiners & Basri reported $Bf = 600 +/-200$ G. However, for the very same star, Shulyak et al. (2017) reported a field strength of $\langle B \rangle = 1400 +/- 200$ G; the discrepancy is possibly due to the use of different line-fitting methods. If a similar discrepancy could be shown to hold for Tr-1, perhaps a measurement of the field of Tr-1 using the approach of Shulyak et al. (2017) might also result in an increase in field strength from 600 (Reiners & Basri 2010) to 1400 G. It is also important to note that, in their modeling of the line profiles, Shulyak et al. (2017) assumed that the magnetic field is dominated by its radial (i.e., vertical) component; this is the component which, according to our mode, has a strength of 1450–1700 G in order to replicate the empirical radius of Tr-1.

4.5. Dynamo Action in Tr-1

If our interpretation of $B_{ps} \approx$ 1450–1700 G as the global dipole field on Tr-1 is reliable, it implies a striking contrast between the strength of the polar field of the Sun (6–12 G) and the strength of the polar field of Tr-1: the latter exceeds that of the Sun by a factor φ of order 100–300. Interestingly, this range overlaps with the prediction in Section 2 above, where, based on Kippenhahn's scaling between dynamo field strength and the angular velocity of the star, we predicted φ could have a value of as much as 160.

The Babcock (1961) dynamo model was developed as an explanation for the solar cycle, but it may also operate in other stars. Let us consider an application to Tr-1. Given that the poloidal field in Tr-1 is 100–300 times stronger than that in the Sun, should we then conclude that dynamo operation will lead to toroidal fields in Tr-1 that are also 100–300 times stronger than the toroidal fields in the Sun? If the answer were yes, it would lead us to conclude that, instead of field strengths of several kG in sunspot umbrae (as in the Sun), the spots on Tr-1 might have umbral field strengths of up to 10^6 G. Such fields would be greatly in excess of the equipartition field strengths in the photosphere of Tr-1 and therefore seem unlikely. In fact, given that the photospheric gas pressures in Tr-1 are $\sim 2 \times 10^6$ dyn cm^{-2}, the equipartition fields are expected to be of order 7 kG. Remarkably, this is close to the maximum value of the photospheric field strengths that have been reported for low-mass stars (Berdyugina et al. 2017; Kochukhov & Lavail 2017; Shulyak et al. 2017). Thus, although in the Sun, the differential rotation leads to a toroidal field that can be stronger than the poloidal field by a factor of $\theta \sim$ several hundred, our results suggest that this simply cannot be the case in Tr-1. The toroidal field in Tr-1 is limited to a maximum strength that is larger than the poloidal by a factor of no more than $\theta \sim$ 4–5. It is possible that the length of the 11 yr activity cycle in the Sun is determined by the time required for differential rotation to enhance the field strength by a factor of $\theta \sim$ several hundred (Mullan 2009). If this possibility also applies to Tr-1, then the activity cycle could be considerably shorter in Tr-1 than in the Sun (if the differential rotation is comparable).

5. Magnetic Fields on the Surface of Tr-1: Consequences for Flares

Now that our models have yielded an estimate of the field strength on the surface of Tr-1, we turn to a consideration of how these results are pertinent to the analysis of the flares that have been detected by the *Kepler* spacecraft.

Flare data for Tr-1 from *Kepler* have been analyzed by Vida et al. (2017) and Paudel et al. (2018a). The energies of individual flares have been quantified by comparing the flare light curves to the quiescent flux. It appears that, at a given flare frequency, the flare energies obtained by Vida et al. differ from those of Paudel et al. by factors of 2–3. Vida et al. assumed that the quiescent flux follows a blackbody curve with temperature 2550 K, whereas Paudel et al. relied on more empirical spectra for the quiescent flux. In the latter case, strong molecular absorption in the visible band reduces the stellar flux at those wavelengths below the blackbody curve by factors of 2–3. As a result, it is not surprising to find that the flare energies estimated by Paudel et al. are smaller by factors of 2–3 than those obtained by Vida et al.

According to Paudel et al. (2018a), flares with optical energies up to a maximum value of (2–3) $\times 10^{32}$ erg have been detected on Tr-1. Since flare energy is related to a combination of flare volume and change in magnetic energy, $E \approx V \Delta B^2 / 8\pi$, we can ask: is it possible to separately estimate the values of ΔB^2 and V in flares?

Of course, in the case of the Sun, separate estimates of B and V are possible: imaging data allow us to determine V, and B can be estimated by combining optical and radio data. (The value of B sets an upper limit on ΔB^2.) But in Tr-1, this separation is not possible. However, as it happens, the largest solar flares among a sample of 400 events detected by the *Solar Dynamics*

Observatory (*SDO*) were recorded to have thermal energies of up to (2–3) $\times 10^{32}$ erg (Aschwanden et al. 2015), coincidentally equal to the maximum flare energy reported by Paudel et al. (2018a) in Tr-1. Might this coincidence in largest flare energy imply that similar processes are at work in solar flares as in flares on Tr-1? Not necessarily. The maximum linear extent of solar flares is observed to be $L \approx 4 \times 10^9$ cm (Aschwanden et al. 2015), i.e., only about 6% of the solar radius. Flares on the Sun are confined to the active regions in which they occur, and even the largest active region on the Sun occupies only a small fraction of the solar surface. The associated maximum solar flare volume ($V \approx 10^{29}$ cm$^3 \approx L^3$; Aschwanden et al. 2015) is less than 0.1% of the solar coronal volume. In this small coronal volume of a solar flare, where the local magnetic field is at most 300–400 G (Aschwanden et al. 2014), the maximum available magnetic energy (assuming the extreme case where all magnetic energy is converted into flare energy, i.e., $\Delta B^2 = B^2$) is $E \approx VB^2/8\pi$. Inserting values, this leads to upper limits on flare energy of (4–6) $\times 10^{32}$ erg; these are indeed adequate to power the observed thermal energies of the largest *SDO* flares.

Suppose we were to apply the solar analogy to flares on Tr-1. If the linear extent of a flare on Tr-1 were to be confined to only 6% of the stellar radius ($=0.121\, R_\odot \approx 8.5 \times 10^9$ cm for Tr-1), then the flare would have a linear extent $L \approx 5 \times 10^8$ cm and a volume of order $L^3 \approx 10^{26}$ cm^3. To power a flare with energy (2–3) $\times 10^{32}$ erg (such as the largest flare reported by Paudel et al. 2018a) from such a volume, the field in the flaring volume, even in the extreme case $\Delta B^2 = B^2$, would have to be as strong as 7 kG. We have already seen (Section 4) that fields of this magnitude may very well exist in the photosphere of Tr-1, but such fields are not relevant for flares. Only in the corona are densities low enough to be conducive to the onset of the instability that can lead to the process of reconnection.

How strong might the coronal fields be in Tr-1? Our results (Section 3 above) suggest that Tr-1 has a global dipole field with a surface strength of 1.45–1.7 kG at the poles; such a field, falling off radially according to r^{-3}, would have a strength of $B_d \approx 200$ G in the corona at a height $h = 1\ R_*$ above the surface. The next higher-order multipole (quadrupole), falling off as r^{-4}, would create coronal fields that are weaker than on the surface by a factor of 16 at height h. Even if the surface strength had its extreme magnitude (7 kG), the quadrupole field B_q would contribute no more than ≈400 G to the field at coronal height $h = 1\ R_*$ above the surface. More likely, the higher multipole would contribute less than 400 G, perhaps 200 G. In such a case, if the lowest and next-lowest multipoles contribute fields that are randomly oriented relative to each other, the total field strength B_t at a height $h = 1\ R_*$ above the surface could be of order $B_t \approx \sqrt{(B_d^2 + B_q^2)} \approx 300$ G. Higher-order multipoles would contribute weaker fields at height h. Thus, at coronal height h, the poloidal field might contribute magnetic energy in the possible flare volume that would be comparable to that contributed by the toroidal field. With a total coronal field of order 300 G, the volume needed to power a flare with an energy of (2–3) $\times 10^{32}$ erg would be of order 8×10^{28} cm^3. The linear extent of such a volume would be of order 4–5 $\times 10^9$ cm. This is a sizable fraction (50%) of the stellar radius of Tr-1 and is much larger than the solar analogy estimated above (where the linear extent amounted to only 6% of the radius). If these estimates have any relevance to stellar flares, they suggest that, whereas solar flares are confined to volumes that are small compared to the volume of the parent star itself, this may not be true in the case of the largest flares on Tr-1.

If the poloidal fields do indeed contribute to the largest flares on a low-mass star, whereas toroidal fields dominate in the smaller flares, then the flare frequency distributions for low-mass stars might obey different laws: one power law for the toroidal flares and another for the poloidal flares. It remains to be seen whether this proposal has any observational signature.

6. Global Field Structure in Stars of Different Spectral Types

The discussion in Section 5 above was based on an attempt to infer certain features of the global field in Tr-1 using the properties of the global field in the Sun for guidance. The conclusions that were drawn in Section 5 are therefore expected to be reliable to the extent that we may consider the global topologies of a G2 dwarf and an M8 dwarf as being (at least somewhat) comparable.

At first sight, it might appear rather unlikely that comparable topologies would exist in such structurally different stars. After all, the dynamo in the Sun almost certainly relies on an $\alpha\Omega$ dynamo in the tachocline (between the radiative core and convective envelope), whereas Tr-1 (which is completely convective) cannot have an $\alpha\Omega$ dynamo and must rely on a different mechanism to generate its magnetic fields, possibly a turbulent (α^2) dynamo (Durney et al. 1993).

If the distinction between stars with or without a tachocline carried over in a one-to-one manner to dynamo operation, we might expect to observe a change in coronal emission (which is magnetically driven) at the transition to complete convection (TTCC; at spectral type M3; Houdebine & Mullan 2015; Houdebine et al. 2017). We might also expect to observe a clear change in magnetic topology at the TTCC as well. However, the observations do not confirm these expectations. First, there is no observable change in coronal emission intensity at spectral type M3 (Fleming et al. 1993). Second, cool dwarfs exhibit a variety of magnetic topologies (Morin et al. 2010): some have fields that are strong and axisymmetric (i.e., poloidal), others have weak fields that are not axisymmetric, and still others have fields that include a toroidal component. In a remarkable plot (their Figure 15), Morin et al. demonstrated that among completely convective stars, one group exhibits a high degree of axisymmetry in their fields, while another group of stars (also completely convective) has fields that are nonaxisymmetric; there are roughly equal numbers of stars in both groups. Also, among stars with radiative cores, Morin et al. found a mixture of stars with axisymmetric and nonaxisymmetric topology, again with roughly equal numbers in both groups. The data suggest that dynamo operation in cool stars leads to a mixture of field topologies, whether the star is completely convective or has a radiative core. The mixture of topologies might be due to bistability (Gastine et al. 2013) or might occur because the dynamo enters an oscillatory mode (Kitchatinov et al. 2014).

It would help if theories of the dynamo could present clear-cut guidance as to how best to proceed in interpreting the stellar data. Unfortunately, theoretical dynamo models contain enough complexities that they lead to a bewildering array of possibilities. Exempli gratia, in the Babcock (1961) solar dynamo, an essential role is played by differential rotation in the surface layers of the Sun. Inclusion of differential rotation

in a dynamo model for a completely convective star led Dobler et al. (2006) to conclude that the dynamo-generated fields in stars would have the property of axisymmetry. However, differential rotation of the solar type need not exist in all cool stars; in fact, in the M3.5 dwarf V374 Peg, evidence suggests that there is no differential rotation on the surface (Morin et al. 2008; Vida et al. 2016). In view of this, rigid-body rotation was included in dynamo models computed by Kueker & Ruediger (1999) and Yadav et al. (2015). In the former, an α^2 dynamo generated nonaxisymmetric fields (resembling a tilted dipole), whereas in the latter, the dynamo generated a dipole-like (i.e., axisymmetric) field.

As regards the possibility of an oscillatory dynamo in any particular star, we would expect to see an activity cycle in that star. Certainly, the Sun undergoes such a cycle, with a period of roughly 11 yr. Is there evidence that low-mass stars have activity cycles? Perhaps; Savanov (2012), Vida et al. (2013), and Reinhold et al. (2017) may be cited in this regard. Savanov (2012) analyzed data for 31 M dwarfs spanning intervals of 2000–3000 days. Activity cycles were reported with periods ranging from less than 1 to almost 10 yr. Interestingly, the cycle periods were found to be independent of rotational period. The author noted that this conclusion "differs significantly" from the results of earlier studies of non-M dwarfs, perhaps indicative of different dynamo modes. Vida et al. (2013) reported on four stars with fast rotation with spectral types ranging from K3 to M4. Three of the stars showed activity cycles with periods of 1–2 yr, but the M4 star in their sample showed no evidence of periodicity. Vida et al. claimed that the absence of long-term cyclic behavior in their M4 star "is consistent with the properties of an α^2 dynamo" at work in that completely convective star. However, in at least one other completely convective star, Savanov (2012) reported that periodic activity was in fact present. Reinhold et al. (2017) reported that 3000 of the 100,000+ stars in the original *Kepler* field undergo variations that could be due to cycles with periods in the range 0.5–6 yr. To be sure, Reinhold et al. did not draw any particular attention to the M dwarfs, so it is not yet clear how much overlap there is between their results and stars with $T_{\rm eff}$ in the range of interest to us here. As far as we know, Tr-1 has not been proven to exhibit an activity cycle, so we cannot yet say whether or not Tr-1 shares this characteristic with the Sun.

In view of the empirical mixture of magnetic topologies among stars of comparable mass, it is difficult at the present time to identify any clear correlations between the magnetic properties of stars and their location relative to the TTCC. From this perspective, despite the significant differences in internal structure between the Sun and Tr-1, dynamo activity apparently leads to magnetic topologies that, from an empirical standpoint, may not differ so much that we are definitively precluded from making legitimate comparisons.

In one regard, however, the results of the present paper may be considered to receive some support from the work of Morin et al. (2010). Inspection of Figure 15 in Morin et al. (2010) suggests that the stars with the strongest fields (with magnetic fluxes of up to 1–2 kG) lie preferentially below the TTCC (i.e., later than M3), while the fields in general become weaker as we examine stars above the TTCC, i.e., stars with masses approaching the mass of the Sun (where magnetic fluxes are of order tens of G). This feature is consistent with our conclusion in the present paper that the polar field (1–2 kG) on the M8 dwarf Tr-1 is significantly stronger (by ∼100) than the polar field in the Sun.

7. Is a Planet in the HZ of Tr-1 Unsuited for Life? CME Effects

Sagan (1973) proposed that flares are harmful to life because of UV photons; we will consider Sagan's argument in Section 7. In this section, we consider a different hazard that could also adversely affect life on exoplanets in orbit around a flare star. Coronal mass ejections (CMEs) are a well-studied aspect of magnetic activity in the Sun; in 1996–2010, the *SOHO* spacecraft recorded 12,433 CMEs (Youssef 2012), i.e., one CME in about 50% of all flares. A CME of sufficient energy may strip the atmosphere from an unprotected (i.e., unmagnetized) planet, so it is relevant to ask: how effective are flare stars at generating CMEs that actually put a planet in peril as regards life?

The answer is not yet clear. The occurrence of a CME-like phenomenon has been reported in at least one flare star (the cool component of V471 Tau) with a spectral type of K2 (e.g., Bond et al. 2001); such a star is similar to the Sun in showing evidence that flares occur in the vicinity of spots (Young et al. 1983). As regards CMEs in an M dwarf, Vida et al. (2016) reported on their detection of moving material reminiscent of a CME in the M4 star V374 Peg; however, the motions involved material falling back to the star, which led Vida et al. (2016) to label two events as "failed CMEs," while a third event was considered a "real" CME. They reported a CME rate that is "much lower than expected from extrapolations of the solar flare–CME relation." Moreover, a variety of observational evidence indicates that CME events in M dwarfs with material clearly moving faster than escape speed are rare. Thus, Leitzinger et al. (2014) used Hα to search for flares and CMEs in 28 dK–dM stars in a young cluster; although flares were observed, they detected "no distinct indication" of CMEs. And Korhonen et al. (2017) examined archival Hα spectra for 40 single active stars but found no CMEs except in the one event reported by Vida et al. (2016). Korhonen et al. (2017) also observed G-K-M stars in five clusters with a range of ages. In four clusters, some flares were detected, but no CMEs. In one cluster, one early-M star showed variability in Hα that might be related to a CME. In conclusion, they wondered, "Maybe we are not detecting many CMEs because there actually are only few of them?" As regards radio evidence for the relative rarity of CMEs from flare stars, we note that Crosley & Osten (2018) conducted a 64 hr long search for evidence of CMEs ejected by an active flare star (EQ Peg; a binary with spectral types M4 and M5). Relying on evidence of Type II radio bursts (drifting from high to low frequencies as a shock wave propagates outward through the corona), the search failed to yield evidence of such features. The authors concluded that their result "casts serious doubt on the assumption that a high flaring rate (in an M dwarf) corresponds to a high rate of CMEs." Moreover, Villadsen & Hallinan (2018), who obtained radio data for five active M dwarfs over 58 hr and detected frequent bursts of coherent emission, found no evidence for analogs of Type II bursts "which are often driven by super-Alfvenic CMEs." Thus, the observed frequency of stellar CMEs is apparently not consistent with naively scaling from the solar case.

Based on the results we have obtained in the present paper, we would like to point out a possible reason for the lack of

CMEs in an active flare star (such as EQ Peg or Tr-1): 3D MHD modeling of CMEs has shown (Alvarado-Gomez et al. 2018, hereafter AG18) that if a star has a "strong enough" global dipole field, a CME with a certain kinetic energy (KE) originating in the low corona may be trapped by the overlying dipole field and unable to escape from the star. Such CMEs would pose no peril to a planet in the HZ. How strong is "strong enough"? For the largest solar-like CMEs, where the KE has been observed to as large as $\sim 3 \times 10^{32}$ erg, AG18 found that a global dipole with a critical strength of $B_c = 75$ G is sufficient to suppress the escape of such CMEs. Since flares on Tr-1 have energies that are observed to extend up to $\sim 3 \times 10^{32}$ erg (Paudel et al. 2018a), CMEs of comparable energy might be associated with the observed flares. In such a case, it does not seem implausible to expect that the suppression of CME escape reported by AG18 for the Sun could also apply to all of the flares that have (so far) been observed on Tr-1, provided that the global dipole in Tr-1 had a strength of at least 75 G. This is where the results of our magnetoconvective models come into play: our modeling in this paper indicates a global dipole field of 1450–1700 G on Tr-1, and these field strengths are well in excess of the 75 G limit discussed by AG18. Therefore, the fields we have derived for Tr-1 can be expected to have the capacity to readily suppress any "solar-like" CMEs on Tr-1 with energies up to the largest values that occur in observed flares.

To be sure, the AG18 models also consider the possibility that a star may occasionally generate CMEs with KE larger than 3×10^{32} erg; such events (which they label as "monster" CMEs) are assigned a KE as large as 10^{34-35} erg. There is no record that the Sun has experienced flares with energies in excess of 10^{33} erg over the past 2000 yr (Maehara et al. 2012). These CMEs of "monster" magnitude have never been reported (so far) in the Sun, nor have flares of such energies been detected in Tr-1 (so far); the maximum flare energy reported by Paudel et al. (2018a) is only $(2–3) \times 10^{32}$ erg. It is true that "superflares" have been reported on solar-like stars with energies $>10^{33}$ erg. Maehara et al. (2012) reported on 365 such events that might possibly enter into the AG18 class of "monster" events. However, among M dwarfs, such as the star we are interested in here, "monster" flares are considerably rarer. For example, Kovari et al. (2007) reported on one flare on an M dwarf with an energy of order 10^{35} erg. Moreover, for a very young brown dwarf, two "monster" releases of optical energy (10^{36-38} erg) have been reported (Paudel et al. 2018b). However, it is possible that the latter events are related to accretion episodes, rather than being magnetic phenomena analogous to bona fide solar-like flares. Besides, even if we know the optical energy released in a "flare," the pronounced rarity of CMEs among detectable stellar flares (see discussion in the second paragraph of this section) means that at present, we seem to have no reliable method to predict the energy associated with a CME that might (or might not) be ejected in connection with any particular flare.

However, if such "monster" events were to occur in the Sun, the models of AG18 indicate that the CME would be able to escape even if the global dipole field were to be of order 75 G. How might this result be applied to Tr-1? From an energetic standpoint, even the "monster" events might be unable to escape from Tr-1 if the coronal field were to be correspondingly stronger: a scaling in which $B_c^2/8\pi \approx$ KE could be plausible. In such a case, the "monster" events modeled by AG18 (with KE $= 10^{34-35}$ erg) could be suppressed in the presence of an overlying dipole field $B_c \approx 750$ G. A crucial aspect of the present paper is that this estimate of B_c is exceeded by the global dipole fields we have obtained for Tr-1. This leads us to hypothesize that all CMEs in Tr-1 (even the "monster" ones) could well be suppressed by the overlying global dipole field that we are suggesting in this paper (1400–1750 G, i.e., $>B_c$). A full modeling effort (which is beyond the limits of the present paper) would be needed to evaluate the correctness of this hypothesis.

To the extent that our hypothesis is correct, we suggest that Tr-1 has a strong enough global field to mitigate (in effect) the CME hazard as regards any life-form that may be struggling to survive on a planet in the HZ of Tr-1.

8. Is a Planet in the HZ of Tr-1 Unsuited for Life? Photon Effects

Since the work of Sagan (1973), it has been believed that UV photons with wavelengths from 2400 to 2900 Å would be harmful to a living cell, especially during solar flares. The flux of UV photons was estimated to be so strong at 2400–2900 Å during a solar flare that a living cell would be subject to a lethal dose in a time interval that would be no longer than 0.3 s. If this conclusion were applicable to Tr-1, the chances of living cells surviving on a planet in orbit around Tr-1 would be small. This result led Vida et al. (2017) to the conclusion that, as regards the planets around Tr-1, the words "unsuited for life?" should be included in the title of their paper.

However, Sagan proposed two methods for protecting the cell from the damaging effects of UV photons. One was to place the cell some tens of meters underwater; such an approach would work on a world provided that water gathers into deep enough ponds (e.g., Pearce et al. 2017). But even if there are no ponds on a planet in orbit around Tr-1, Sagan's second suggestion was to use certain organic molecules (especially the bases that occur in genetic material) to absorb the harmful photons in the outer layers of the cell, preventing them from reaching the genetic material in the nucleus. Thus, UV photons are not automatically harmful to cell life.

In fact, under some circumstances, especially in the vicinity of flare stars, the UV photons from flares may actually be beneficial for the origin of life (Ranjan et al. 2017). Moreover, once life has gotten started on planets that are in orbit around M dwarfs, the visible photons from flares also serve to enhance the efficiency of photosynthesis by as much as an order of magnitude (Mullan & Bais 2018).

In view of these points, we suggest that the effects of flares on life are not necessarily always negative. On the contrary, both of the above photonic processes may play a role in enhancing the probability of life on the HZ planets around the flare star Tr-1.

9. Conclusions

Using a model of magnetoconvection in which the onset of convection in an electrically conducting medium is impeded quantitatively by the presence of a vertical magnetic field, we have obtained a magnetic model of Tr-1 (spectral type M8). Our model includes the effects of finite electrical conductivity, and the results are found to fit all of the available empirical data for Tr-1 (radius, mass, effective temperature, and metallicity). Our models predict that the vertical component of the surface

magnetic field on Tr-1 is in the range ∼1450–1700 G. We argue that this field strength applies to the global dipole field in the photosphere at the magnetic poles. If this argument is valid, the surface field on Tr-1 is stronger than the global dipolar field on the Sun (6–12 G; Hundhausen 1977) by factors of ∼100. This enhancement in field strength may be related to the fact that the angular velocity of rotation of Tr-1 exceeds that in the Sun by factors of 10–30.

Compared to the recent modeling that we have reported on two other flare stars, GJ 65A/B, with spectral types M5.5 and M6 (MacDonald et al. 2018), the surface field on Tr-1 is weaker by a factor of about 2. The weakness of the Tr-1 field compared to that of GJ 65A/B may be related to the slower rotation of Tr-1, which rotates at least 3 times slower than GJ 65A/B. However, both systems are rotating with sufficiently short periods (0.3–0.8 days) that the dynamos in both systems may be saturated. If that is the case, we may simply be seeing the intrinsic scatter of a dynamo in the saturation regime, where empirical field strengths are known to exhibit scatters by factors of 2 (Reiners et al. 2009).

Contrary to a question raised in the title of an article by Vida et al. (2017), we suggest that a planet in the HZ of Tr-1 need not be considered "unsuited for life" despite the occurrence of well-documented flaring activity on the parent star. In fact, we believe that conditions near Tr-1 may even be beneficial for life for the following reasons: (i) the presence of flare photons at certain ultraviolet wavelengths can be beneficial to the origin of the bases required for nucleic acids, (ii) the presence of flare photons at visible wavelengths of 400–700 nm can enhance the efficiency of photosynthesis, and (iii) the strong global magnetic field that we have modeled on Tr-1 may suppress CMEs to the extent that the violent effects of CMEs are less likely to pose a threat of removing the atmosphere of the planet.

We thank an anonymous referee for constructive comments on the paper, especially as regards several valuable citations. J.M. and H.F. acknowledge support from the NASA Delaware Space Grant.

ORCID iDs

D. J. Mullan https://orcid.org/0000-0002-7087-9167
J. MacDonald https://orcid.org/0000-0002-0506-5124

References

Alfvén, H., & Carlqvist, P. 1967, SoPh, 1, 220
Allard, F., Homeier, D., & Freytag, B. 2012a, RSPTA, 370, 2765
Allard, F., Homeier, D., Freytag, B., & Sharp, C. M. 2012b, in EAS Publ. Ser. 57, Low-mass Stars and the Transition Stars/Brown Dwarfs, ed. C. Reylé, C. Charbonnel, & M. Schultheis (Les Ulis: EDP Sciences), 3
Alvarado-Gomez, J., Drake, J. J., Cohen, O., Moschou, S. P., & Garraffo, C. 2018, ApJ, 862, 93
Anders, E., & Grevesse, N. 1989, GeCoA, 53, 197
Antia, H. M., & Basu, S. 2006, ApJ, 644, 1292
Aschwanden, M. J., Boerner, P., Ryan, D., et al. 2015, ApJ, 802, 53
Aschwanden, M. J., Xu, Y., & Jing, J. 2014, ApJ, 797, 50
Asplund, M., Grevesse, N., & Jacques Sauval, A. 2006, NuPhA, 777, 1
Babcock, H. W. 1961, ApJ, 133, 572
Berdyugina, S. V., Harrington, D. M., Kozmychov, O., et al. 2017, ApJ, 847, 61
Bond, H. E., Mullan, D. J., O'Brien, M. S., & Sion, E. M. 2001, ApJ, 560, 919
Bopp, B. W., & Evans, D. S. 1973, MNRAS, 164, 343
Bray, R. J., & Loughhead, R. E. 1964, Sunspots (New York: Dover), (BL64)
Browning, M. K. 2008, ApJ, 676, 1262
Burgasser, A., & Mamajek, E. 2017, ApJ, 845, 110, (BM17)
Caffau, E., Ludwig, H.-G., Steffen, M., Freytag, B., & Bonifacio, P. 2011, SoPh, 268, 255
Chabrier, G., Gallardo, J., & Baraffe, I. 2007, A&A, 472, L17
Costa, E., Mendez, R. A., Jao, W.-C., et al. 2006, AJ, 132, 1234
Crosley, M. K., & Osten, R. A. 2018, ApJ, 862, 113
Delrez, L., Gillon, M., Triaud, A. H. M. J., et al. 2018, MNRAS, 475, 3577
Dieterich, S. B., Henry, T. J., Jao, W.-C., et al. 2014, AJ, 147, 94
Dmitrienko, E. S., & Savanov, I. S. 2018, ARep, 62, 412
Dobler, W., Stix, M., & Brandenburg, A. 2006, ApJ, 638, 336
Dodd, M. S., Papineau, D., Grenne, T., et al. 2017, Natur, 543, 60
Durney, B. D., De Young, D. S., & Roxburgh, I. W. 1993, SoPh, 145, 207
Feiden, G. A., & Chaboyer, B. 2014, A&A, 571, A70
Filippazzo, J. C., Rice, E. L., Faherty, J., et al. 2015, ApJ, 810, 158
Fleming, T. A., Giampapa, M. S., Schmitt, J., & Bookbinder, J. A. 1993, ApJ, 410, 387
Gastine, T., Morin, J., Duarte, L., et al. 2013, A&A, 549, L5
Gillon, M., Jehin, E., Lederer, S. M., et al. 2016, Natur, 533, 221
Gough, D. O., & Tayler, R. J. 1966, MNRAS, 133, 85, (GT)
Habbal, S. R., Druckmuller, M., Morgan, H., et al. 2010, ApJ, 719, 1362
Hood, A. W., & Priest, E. R. 1979, SoPh, 64, 303
Houdebine, E. R., & Mullan, D. J. 2015, ApJ, 801, 106
Houdebine, E. R., Mullan, D. J., Bercu, B., et al. 2017, ApJ, 837, 96
Hundhausen, A. 1977, in Coronal Holes and High Speed Wind Streams, ed. J. B. Zirker (Boulder, CO: Colorado Assoc. Univ. Press), 299
Kippenhahn, R. 1973, in Stellar Chromosphere, ed. S. D. Jordan & E. H. Avrett (Washington, DC: NASA), 275
Kitchatinov, L. L., Moss, D., & Sokoloff, D. 2014, MNRAS, 442, L1
Kochukhov, O., & Lavail, A. 2017, ApJL, 835, L4
Korhonen, H., Vida, K., Leitzinger, M., et al. 2017, in IAU Symp. 328, Living Around Active Stars, ed. D. Nandy, A. Valio, & P. Petit (Cambridge: Cambridge Univ. Press), 198
Koskela, J. S., Virtanen, I. I., & Mursula, K. 2017, ApJ, 835, 63
Kosovichev, A., & Rozelot, J.-P. 2018, ApJ, 861, 90
Kovari, Z., Vilardell, F., Ribas, I., et al. 2007, AN, 328, 904
Krishna Swamy, K. S. 1966, ApJ, 145, 174, (KS)
Kueker, M., & Ruediger, G. 1999, in ASP Conf. Ser. 178, Stellar Dynamos: Nonlinearity and Chaotic Flows, ed. M. Nunez & A. Ferriz-Mas (San Francisco, CA: ASP), 87
Leitzinger, M., Odert, P., Greimel, R., et al. 2014, MNRAS, 443, 898
Luger, R., Sestovic, M., Kruse, E., et al. 2017, NatAs, 1, 0129
MacDonald, J., & Gizis, J. E. 2018, MNRAS, 480, 1711
MacDonald, J., & Mullan, D. J. 2009, ApJ, 700, 387
MacDonald, J., & Mullan, D. J. 2012, MNRAS, 421, 3084
MacDonald, J., & Mullan, D. J. 2014, ApJ, 787, 70
MacDonald, J., & Mullan, D. J. 2017a, ApJ, 843, 142
MacDonald, J., & Mullan, D. J. 2017b, ApJ, 850, 58
MacDonald, J., Mullan, D. J., & Dieterich, S. 2018, ApJ, 860, 15
Maehara, H., Shibayama, T., Notsu, S., et al. 2012, Natur, 485, 478
Morin, J., Donati, J.-F., Petit, P., et al. 2008, MNRAS, 390, 567
Morin, J., Donati, J.-F., Petit, P., et al. 2010, MNRAS, 407, 2269
Morris, B. M., Agol, E., Davenport, J. R. A., & Hawley, S. L. 2018, ApJ, 857, 39
Mullan, D. J. 2009, Physics of the Sun: A First Course (Boca Raton, FL: CRC Press)
Mullan, D. J., & Bais, H. A. 2018, ApJ, 865, 101
Mullan, D. J., & MacDonald, J. 2001, ApJ, 559, 353
Mullan, D. J., & MacDonald, J. 2010, ApJ, 713, 1249
Mullan, D. J., MacDonald, J., & Townsend, R. 2007, ApJ, 670, 1420
Mullan, D. J., & Paudel, R. R. 2018, ApJ, 854, 14
Paudel, R. R., Gizis, J. E., Mullan, D. J., et al. 2018a, ApJ, 858, 55
Paudel, R. R., Gizis, J. E., Mullan, D. J., et al. 2018b, ApJ, 861, 76
Pearce, B. K. D., Pudritz, R. E., Semenov, D. A., & Henning, T. K. 2017, PNAS, 114, 11327
Rackham, B. V., Apai, D., & Giampapa, M. S. 2018, ApJ, 853, 122
Radick, R. R., Lockwood, G. W., Henry, G. W., Hall, J. C., & Pevtsov, A. A. 2018, ApJ, 855, 75
Radick, R. R., Lockwood, G. W., Skiff, B. A., & Baliunas, S. L. 1998, ApJS, 118, 239
Rajpurohit, A. S., Reylé, C., Allard, F., et al. 2013, A&A, 556, 15
Ranjan, S., Wordsworth, R., & Sasselov, D. D. 2017, ApJ, 843, 110
Reiners, A., & Basri, G. 2010, ApJ, 710, 924
Reiners, A., Basri, G., & Browning, M. 2009, ApJ, 692, 538
Reinhold, T., Cameron, R. H., & Gizon, L. 2017, A&A, 603, A52
Roettenbacher, R. M., & Kane, S. R. 2017, ApJ, 851, 77
Sagan, C. 1973, J. Theor. Biol., 39, 195
Savanov, I. S. 2012, ARep, 56, 716

Schmelz, J. T., Holman, G. D., Brosius, J. W., & Wilson, R. F. 1994, ApJ, 434, 786
Shapiro, A. I., Solanki, S. K., Krivova, N. A., et al. 2014, A&A, 569, A38
Shulyak, D., Reiners, A., Engeln, A., et al. 2017, NatAs, 1, 0184
Spruit, H. C. 1976, SoPh, 50, 269
Strassmeier, K. G. 1999, A&A, 347, 225
Van Grootel, V., Fernandes, C. S., Gillon, M., et al. 2018, ApJ, 853, 30
Vida, K., Kovari, Zs., Pal, A., Olah, K., & Kriskovics, L. 2017, ApJ, 841, 124
Vida, K., Kriscovics, L., & Olah, K. 2013, AN, 334, 872
Vida, K., Kriscovics, L., Olah, K., et al. 2016, A&A, 590, 11
Villadsen, J., & Hallinan, G. 2018, ApJ, submitted (arXiv:1810.00855)
Yadav, R. K., Christensen, U. R., Morin, J., et al. 2015, ApJL, 813, L31
Young, A., Klimke, A., Africano, J. L., et al. 1983, ApJ, 267, 655
Youssef, M. 2012, JAsGe, 1, 172